Geoderma 207–208 (2013) 279–290

Contents lists available at SciVerse ScienceDirect

Geoderma

journal homepage: www.elsevier.com/locate/geoderma

Quantifying mineral abundances of complex mixtures by coupling spectral deconvolution of SWIR spectra (2.1–2.4 μm) and regression tree analysis

V.L. Mulder [a,*], M. Plötze [b], S. de Bruin [a], M.E. Schaepman [c], C. Mavris [d], R.F. Kokaly [e], M. Egli [d]

[a] Laboratory of Geo-Information Science and Remote Sensing, Wageningen University, Droevendaalsesteeg 3, P.O. Box 47, 6700 AA Wageningen, The Netherlands
[b] Institute for Geotechnical Engineering, ETH Zürich, 8093 Zürich, Switzerland
[c] Remote Sensing Laboratories, Department of Geography, University of Zürich, Winterthurerstrasse 190, 8057 Zürich, Switzerland
[d] Physical Geography, Department of Geography, University of Zürich, Winterthurerstrasse 190, 8057 Zürich, Switzerland
[e] U.S. Geological Survey, Denver Federal Center, Denver, CO 80225-0046, United States

ARTICLE INFO

Article history:
Received 6 November 2012
Received in revised form 29 April 2013
Accepted 14 May 2013
Available online 21 June 2013

Keywords:
Soil minerals
Spectral unmixing
Exponential Gaussian optimisation
Regression trees
SWIR reflectance spectroscopy

ABSTRACT

This paper presents a methodology for assessing mineral abundances of mixtures having more than two constituents using absorption features in the 2.1–2.4 μm wavelength region. In the first step, the absorption behaviour of mineral mixtures is parameterised by exponential Gaussian optimisation. Next, mineral abundances are predicted by regression tree analysis using these parameters as inputs. The approach is demonstrated on a range of prepared samples with known abundances of kaolinite, dioctahedral mica, smectite, calcite and quartz and on a set of field samples from Morocco. The latter contained varying quantities of other minerals, some of which did not have diagnostic absorption features in the 2.1–2.4 μm region. Cross validation showed that the prepared samples of kaolinite, dioctahedral mica, smectite and calcite were predicted with a root mean square error (RMSE) less than 9 wt.%. For the field samples, the RMSE was less than 8 wt.% for calcite, dioctahedral mica and kaolinite abundances. Smectite could not be well predicted, which was attributed to spectral variation of the cations within the dioctahedral layered smectites. Substitution of part of the quartz by chlorite at the prediction phase hardly affected the accuracy of the predicted mineral content; this suggests that the method is robust in handling the omission of minerals during the training phase. The degree of expression of absorption components was different between the field sample and the laboratory mixtures. This demonstrates that the method should be calibrated and trained on local samples. Our method allows the simultaneous quantification of more than two minerals within a complex mixture and thereby enhances the perspectives of spectral analysis for mineral abundances.

1. Introduction

Soil mineralogy is an important indicator for soil formation and parent material characterisation. Among other minerals in soils like quartz, feldspars and carbonate minerals, clay minerals are the main secondary phases formed by the weathering of the parent material. The abundance of different clay minerals and their structural features become useful indicators in defining the evolutional stage of a soil (Egli et al., 2008; Hong et al., 2007; Mavris et al., 2011; Sedov et al., 2003). In environmental and geological studies, the characterisation (and quantification) of soil mineralogy is typically achieved using X-ray diffraction (XRD). XRD is broadly acknowledged as the essential tool for mineral determination of mono- or multi-mineral mixtures (Bish and Plötze, 2011; Gomez et al., 2008; Mulder et al., 2011; Omotoso et al., 2006). The basic limitation of XRD is that the analysis must be carried out indoors, basically due to sample preparation requirements and specific laboratory treatments necessary for some clay minerals, such as glycolation and heating after various cation saturations. Visible Near Infrared and Shortwave Infrared (VNIR/SWIR) spectroscopy has proven to be an efficient method for the determination of various soil properties since measurements can be done with little effort and in situ (Ben-Dor et al., 2009; Viscarra Rossel et al., 2006). In this paper, we propose and demonstrate its use for simultaneous quantification of mineral abundances from complex mixtures.

Some minerals such as quartz, and low iron feldspars do not show absorption features in the 0.350–2.500 μm wavelength range except for the features arising from $Fe^{2+/3+}$ related to their weathering products (Clark et al., 1990). Detection of minerals having absorption features within the 0.350–2.500 μm range have been successfully obtained using linear spectral unmixing techniques (Dennison and Roberts, 2003). However, these analyses were limited to estimating the main component within a sample having the most distinct absorption feature (Mulder et al., 2012b). Linear mixing behaviour of spectra, however, is highly unlikely

* Corresponding author. Tel.: +31 317483894; fax: +31 317419000.
E-mail address: Titia.Mulder@wur.nl (V.L. Mulder).

0016-7061/$ – see front matter © 2013 Elsevier B.V. All rights reserved.
http://dx.doi.org/10.1016/j.geoderma.2013.05.011

in soils because the mineral constituents are typically in intimate association with one another. Influencing factors are e.g. the opaqueness of minerals and coating by other minerals. Furthermore, simultaneous retrieval of multiple mineral abundances from reflectance spectra in the 0.350–2.500 μm region is affected by the co-occurrence of absorption features at similar wavelengths arising from overtones and combinations of the fundamental absorptions of OH, H_2O and CO_3 which occur at wavelengths greater than 2.500 μm, nonlinear mixing (or scattering) phenomena (Singer, 1981; Sunshine et al., 1990), and measurement noise (Stenberg et al., 2010). Hence, reflectance spectra of mixtures are typically a complex result from the combinations of the spectral characteristics of the constituents (Clark et al., 1990), as illustrated in Fig. 1. A comparison of the diagnostic features of pure calcite with the continuum removed reflectance (Clark, 1998) of samples containing an spectrally dominant mineral shows that e.g. in the presence of quartz the double absorption feature near 2.300–2.350 μm is present but much less distinct while it is absent in mineral mixtures of calcite with kaolinite or dioctahedral mica at approximately 15% abundance. Note also that the absorption near 2.150 μm is absent in the smectite and dioctahedral mica mixtures while it changes the typical absorption of kaolinite. Depending on the composition, the abundance and the spatial arrangement of the minerals, the total reflectance resulting from the scattering of the minerals within the intimate mixture produces positional shifts, changes in intensity, disappearance of absorption features or changes in their shape.

Methods aiming to match diagnostic absorption features with spectra from a large spectral library include the Tetracorder (Clark et al., 2003) and the CRISM Analysis Tool (CAT) (Flahaut et al., 2012). While the extended library enables application to unknown areas without the need of calibration on local samples, the retrieval of the mineral composition of complex mixtures remains limited because spectral mixing effects may yield diagnostic features not distinct enough to be matched to minerals in the spectral library. Theoretically the spectra could be matched to the corresponding spectra with known abundances in the library. However the spectra to be included in the library of various minerals and the possible variation in mixtures of these would follow combinatory logic (Mulder et al., 2012b). So, the methods are commonly applied to characterising mineral composition in terms of presence or absence but not quantifying mineral abundances (Clark et al., 2003). Non-linear models, such as the single scattering albedo model of Hapke (Hapke, 2002; Warell and Davidsson, 2010) have been successful in predicting the abundances of minerals in intimate mixtures. The main reason why such a nonlinear approach is not widely adopted is the amount of detailed information on the scattering properties of all endmembers needed to perform the calculations (Keshava and Mustard, 2002). Alternatively, the modelling of reflectance and the inference of absorption components within complex features can be done by fitting Gaussian curves or modified Gaussian curves to the absorption features and absorption components in reflectance spectra of minerals also referred to as spectral deconvolution (Burns, 1993; Noble et al., 2006; Roush and Singer, 1986; Singer, 1981). Sunshine et al. (1990) provided the explanation for Gaussian behaviour of absorption features. The signal sensed by a spectrometer corresponds to the mean response from massive amounts of electronic and vibrational processes that cause absorption around specific wavelengths (absorption bands). Owing to the Central Limit Theorem, an absorption feature closely resembles a Gaussian distribution. Alternatively, the exponential Gaussian optimisation (EGO) of Pompilio et al. (2009) has been designed to model absorption components which are not Gaussian in shape and accounts for saturation and asymmetry effects. The use of such a quantitative deconvolution method for a spectrum of a specific composition is dependent only on the spectra and absorption of the minerals themselves rather than the detailed information on the scattering properties required for the Hapke model (Shepard and Helfenstein, 2007). It provides the means to study the individual absorption components in spectra and interpretation of these can then be analysed in terms of composition (Sunshine et al., 1990).

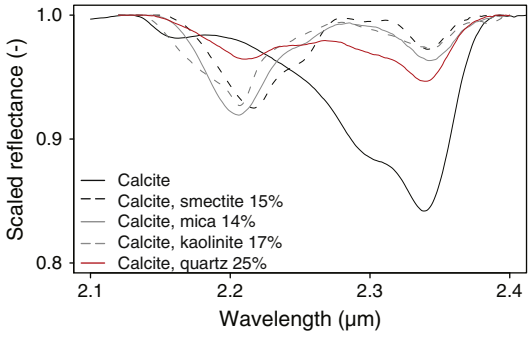

Fig. 1. Continuum removed reflectance of calcite and mixtures containing calcite. The mixtures contain minerals of which the additional mineral with absorption features has an abundance of approximately 15% and a sample of calcite with 25% quartz (spectra originate from field samples measured in this experiment, the calcite spectra contain a small trace of mica).

Modified Gaussian models have been demonstrated in laboratory experiments by mixtures with two constituents of interest using either multiple linear regression techniques (Bishop et al., 2011; Singer, 1981) or the ratio between intensities of absorption components (Kanner et al., 2007; Sunshine and Pieters, 1993). It has thus been assumed that the model parameters vary as a linear function of the relative proportions of the constituents in the mixture (Pompilio et al., 2009; Sunshine and Pieters, 1998). Samples with similar mineralogy but unknown abundance can then be predicted by the calibrated mixtures models. However, such approach is insufficient for the prediction of mixtures with more than two minerals. Model parameters might vary linearly over a short range of the mixture possibilities but over the complete range of mixture possibilities, non-linearity dominates. As a result, a different type of analysis is required to relate the EGO parameters to the mineral content in order to determine abundances of three or more minerals within a mixture. We propose a recursive partitioning of the data by regression tree analysis (Breiman et al., 1984). Regression tree analysis allows to deal with nonlinearity and interactions between the EGO parameters. Regression trees can be trained by setting decision rules based on the predictive structure of the dataset with mineral mixtures (Breiman et al., 1984). This approach is an often used data mining technique in several disciplines (De'Ath and Fabricius, 2000; McBratney et al., 2003; Yang et al., 2003).

Below we give details on combining the deconvolution by EGO and the use of regression trees on the EGO parameter values for quantifying mineral abundances of mixtures having more than two constituents. The approach is demonstrated on a range of prepared samples with known abundances of kaolinite, dioctahedral mica, smectite, calcite and quartz and on a set of field samples from Morocco, which were quantitatively analysed by XRD analysis.

2. Methods

2.1. Spectral deconvolution by Gaussian modelling of absorption components

Deconvolution of the spectra by fitting Gaussian curves needs to be concerned with partly overlapping absorption components (Sunshine and Pieters, 1993) as well as the presence of amorphous materials and impurities that may modify absorption band shapes and contribute to saturation and asymmetry of spectral features (Burns, 1993; Pompilio et al., 2009). The Modified Gaussian Model (MGM) describes absorption components as modified Gaussian distributions that are parameterised by a band centre, band width (full width at half maximum) and band strength (amplitude intensity), for more details see Sunshine et al. (1990) and Kanner et al. (2007). In several studies MGM has been successfully used to model overlapping absorptions components (Bishop et al., 2011; Kanner et al., 2007; Lane et al., 2011; Ogawa et al., 2011; Pinet

et al., 2007; Sunshine and Pieters, 1993, 1998). Because we have mineral mixes with many constituents, the absorption components may be modified in shape due to saturation and asymmetry effects. It is important to include a parameter on saturation. When saturation occurs the absorption band is reduced in depth and becomes flatter near the minimum. Without information on saturation the spectral deconvolution might be less accurate because it cannot discriminate between overlapping and saturated absorption bands (Pompilio et al., 2009). Therefore, the deconvolution of the spectra will be performed with the exponential Gaussian optimisation (EGO) of Pompilio et al. (2009) to model those absorption components which are not Gaussian in shape and account for saturation and asymmetry effects.

The EGO algorithm of Pompilio et al. (2009, 2010) first fits a continuum linear in wavelength over the isolated absorption feature and secondly fits the feature's individual absorption components by a number of EGO profiles in log reflectance. These are then combined into the final fitted curve of an isolated feature. The continuum over the isolated feature is set according to Eq. (1):

$$C(\lambda) = c_0 + c_1\lambda^{-1} \quad (1)$$

where c_0 is the offset and c_1 a constant for the slope of the continuum and λ is the wavelength (Sunshine et al., 1990). In wavelength space, the continuum becomes a flat line in infrared and a curved line at shorter wavelengths (Clénet et al., 2011). Then, for each absorption component an EGO profile is described, using the five parameters position, intensity, width, band saturation and asymmetry (Eq. (2)):

$$\mathrm{EGO}(\lambda) = -\frac{s}{1-e^{-0.5t}}\left[1-e^{-0.5\left(te^{-0.5\left(\frac{\lambda-\mu}{\sigma+k(\lambda-\mu)}\right)^2}\right)}\right] \quad (2)$$

where λ represents the wavelength in micrometres [μm], s the band amplitude intensity, μ the centre and σ the full width at half maximum (FWHM) of the EGO profile. The parameter t is used to model band saturation, and k is the coefficient for asymmetry.

The complete model algorithm is described by the fitted continuum $C(\lambda)$ and the sum of the different EGO profiles superimposed onto the continuum (Eq. (3)):

$$\ln(R(\lambda)) = C(\lambda) + \sum \mathrm{EGO}(\lambda) \quad (3)$$

where R is the reflectance spectrum as a function of the wavelength, $C(\lambda)$ indicates the continuum as a function of wavelength and EGO (λ) are the individual profiles fitted to each absorption feature again as a function of wavelength. Log transformed reflectance is used since absorption is assumed having a logarithmic dependence between transmissivity of light through a substance and the product of the path length and the absorption coefficient of the substance (Beer–Lambert law) (Sassaroli and Fantini, 2004). The appropriate number of absorption components to be used in the EGO analysis depends on the number of known minerals present in the material mixture and the number of unique electronic and vibrational absorptions for each mineral (Kanner et al., 2007). For a graphical demonstration of the EGO algorithm we refer to the work of Pompilio et al. (2009, 2010).

We used a similar approach as Pompilio et al. (2009, 2010) to evaluate the deconvolution of the spectra. So called *best fit* models were assessed using the root mean squared error (RMSE) of the estimated natural log of reflectance. Based on visual interpretation, additional EGO profiles were included at subsequent iterations when the current set of profiles did not achieve a proper fit in specific wavelength ranges. These EGO profiles were centred around the position (μm) of the selected absorption components, as discussed in Section 2.3.1. A best fit of the estimated natural log reflectance results from negligible improvement of the corresponding RMSE with subsequent iterations. For a complete description of the statistics we refer to Appendix A in Pompilio et al. (2009).

The EGO routine was implemented within the R-environment by Pompilio et al. (2009), (R Development Core Team, 2011). The approximation of the parameters is obtained by optimisation of the parameters in the model aiming for the least RMSE using a Levenberg–Marquardt approach (Garbow et al., 1980; Moré, 1978; Press et al., 1992, and references therein).

2.2. Determination of mineralogical composition by regression trees

Regression tree analysis (RTA) is a flexible method for specifying the conditional distribution of a variable y, given a vector of predictor variables X (Breiman et al., 1984). The goal of the regression tree is to create relatively homogeneous subsets. This is done by recursively partitioning the data in binary splits based on a single predictor variable. The partition is determined by splitting rules, evaluating the best split at each internal node with respect to homogeneity of the two subsets. Each observation is ultimately assigned to a unique terminal node based on the splitting rules set for each node in the tree (Breiman et al., 1984).

In this work, mineral abundance was predicted by coupling RTA with the EGO results whereby a separate regression tree was trained for the individual minerals. In the first instance, a maximum tree was grown to the point where additional splits could not be made due to lack of data, using the EGO profile parameters for the corresponding mineral as the predictor variables. Subsequently, the least important splits were removed by pruning the tree based upon the standard error of the estimate from cross-validation. The optimal tree was derived by using the so called 1 *SE* rule, introduced by Breiman et al. (1984). By this rule we select the simplest tree where the error estimate is within one standard error of the lowest error of the estimate. Thereby we reduce the instability of the model and also the number of parameters used for the prediction model. In addition, the stopping rules used for training of the trees included (Breiman et al., 1984); the minimum number of observations that must exist in a node in order to be considered for a split were set to 3 for the laboratory experiment and to 5 for the field experiment; a split was accepted if the overall coefficient of determination (R^2) of leave-one-out cross validation increased at each step by at least 0.01.

An additional validation was done to test the model performance with a number of samples which were not included for training of the trees. By setting aside 16 randomly selected samples from the field experiment (total 77 samples), training of the trees was based on the remaining samples. The accuracy of the predicted mineralogy from the cross validation and the external validation was assessed by the coefficient of determination (R^2) from the cart analysis and the root mean square error (RMSE) of the predicted mineral abundances compared to the known mineralogy. Calculations were performed using the "R language and environment for statistical computing" version 2.14.1 (R Development Core Team, 2011) and the contributed package *rpart* (Ripley, 2011). For more details about RTA we refer to Breiman et al. (1984).

2.3. Case studies

2.3.1. Laboratory experiment

2.3.1.1. Mineral samples. The laboratory experiment was conducted on spectra of physical mixtures of almost pure minerals. The minerals included in the mixtures were kaolinite, dioctahedral mica (illite), smectite, calcite and quartz, those found to be dominantly present in the study area (see Section 2.3.2). Since quartz was ubiquitous in the study area a fixed amount of quartz was added to each sample. Quartz is known to lack absorption features in the studied wavelength range. Nevertheless, inclusion of quartz in physical mixtures

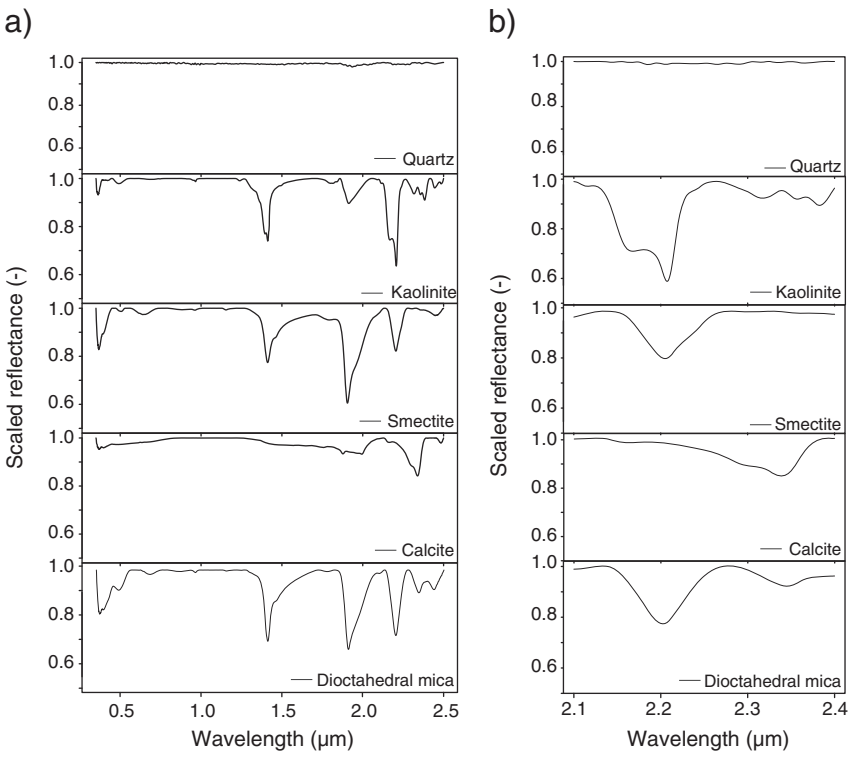

Fig. 2. Continuum removed spectra from the pure minerals in this study, right: full VNIR/SWIR, left: between 2.1 and 2.4 μm (spectra originate from samples measured in this experiment).

is important because of potential secondary impact, from scattering of light by quartz, on the absorption features of other minerals (Clark, 1999); however, in this study the direct estimation of quartz abundance using EGO and regression tree analysis is not supported because of absence of absorption features (see also Fig. 2). The minerals were obtained either from Clay Minerals Society (CMS) source clay repository (kaolinite KGa-2 Georgia U.S.A., Fe-chlorite CCa-1 California U.S.A.) or are industrial products (quartz and calcite from Fluka, illite sarospatakite from Füzerradvany Hungary, and montmorillonite cloisite–Na from Southern Clay Products U.S.A.). A dataset of 35 samples was used for training the regression trees. To obtain the required opacity for the spectral measurements each sample had a gravimetric content of 15 g.

Samples 1–25 consisted of gravimetric, intimate mineral mixes of pure kaolinite, dioctahedral mica, smectite, calcite and quartz with a grain size of <63 μm. Each of these samples had a quartz content of 25 wt.%, while the other minerals contributed to the remaining 75 wt.% with abundance as indicated in Table 1. A pure sample of each mineral was included as reference for the absorption characteristics of the pure minerals. With this laboratory experiment the true composition of the sample can be assumed to be known and the chance that there are unknown minerals influencing the model performance is minimised.

A sensitivity test was done to test the model performance against the presence of an unknown mineral on which the regression trees were not trained. Missing specific absorption components might reduce the statistical relationship between the EGO profiles and mineral contents included in the analysis. Therefore, in five samples chlorite was admixed, which is another common sheet silicate in soils (Dalton et al., 2004).

2.3.1.2. Spectral measurements and reflectance of minerals. Spectral measurements were performed under laboratory conditions with an Analytical Spectral Devices (ASD) Fieldspec 3 spectroradiometer. The spectroradiometer covered the 0.350–2.500 μm wavelength region with a resolution of 3 nm at 700 nm and 10 nm at 1400/2100 nm (1.4 nm and 2 nm sampling interval). The samples were measured using an ASD High Intensity Muglight (4 W quartz tungsten halogen lamp) to minimise measurement errors associated with stray light and specular reflection from the minerals. The powdered samples were placed in pure quartz sample holders to avoid scattering from the sample holder, since quartz lacks distinct absorption features in the measured wavelength region. All sample holders were calibrated against a non-reflecting reference standard prior to sample measurements.

The reflectance of pure minerals — including those studied in this paper — was extensively reviewed by Clark et al. (1990) and Swayze et al. (2003). Fig. 2 presents the continuum removed (CR) spectra of the pure minerals; the spectra show clearly the strong absorption features of water around 1.400 μm and 1.900 μm, related to the overtones and combinations of the fundamental vibrational characteristics of water as well as absorption from the OH bends. The diagnostic characteristic of kaolinite is the double absorption feature around 2.150 μm and 2.200 μm; Dioctahedral mica has two primary absorption features centred around 2.200 μm and 2.350 μm. Smectite contains water in the crystal structure and therefore exhibits strong absorption near 1.400 μm and 1.900 μm. In the SWIR, it can be recognised by the single sharp and symmetrical absorption at 2.200 μm due to the AlOH bend and the smaller absorption around 2.250 μm. For calcite, second and third overtones and combinations of the CO_3 fundamentals occur in the near IR. The two strongest absorptions are found at 2.500–2.550 μm and 2.300–2.350 μm. Three weaker absorption bands occur near 2.120–2.160 μm, 1.970–2.000 μm and 1.850–1.870 μm. In the SWIR region, calcite is distinguished from the other minerals by the weaker absorption near 2.120–2.160 μm and the double absorption feature near 2.300–2.350 μm (Clark et al., 1990). Based on the bends which discriminate the minerals from each other we study the wavelength range between 2.100 and 2.400 μm. Within this wavelength range quartz does not have any absorption feature. Direct estimation of quartz abundances using EGO and regression tree analysis is therefore not supported. As indicated earlier it is important to include quartz into the mixtures. The

Table 1
Overview of prepared mineral samples, content is given in wt.% of the total mass of 15 g.

Sample no.	Smectite	Kaolinite	Dioctahedral mica	Calcite	Quartz	Chlorite
1	10	5	40	20	25	0
2	45	15	15	0	25	0
3	5	5	50	15	25	0
4	20	10	10	35	25	0
5	10	15	15	35	25	0
6	0	0	60	15	25	0
7	10	15	40	10	25	0
8	45	20	5	5	25	0
9	25	15	30	5	25	0
10	0	10	40	25	25	0
11	20	15	25	15	25	0
12	15	10	20	30	25	0
13	5	5	55	10	25	0
14	0	0	20	55	25	0
15	0	0	0	75	25	0
16	60	5	10	0	25	0
17	50	10	5	10	25	0
18	15	0	30	30	25	0
19	0	20	55	0	25	0
20	0	0	50	25	25	0
21	15	10	35	15	25	0
22	5	0	35	35	25	0
23	15	5	20	35	25	0
24	50	5	20	0	25	0
25	10	0	45	20	25	0
Pure minerals						
26	100	0	0	0	0	0
27	0	100	0	0	0	0
28	0	0	100	0	0	0
29	0	0	0	100	0	0
30	0	0	0	0	100	0
Addition of chlorite[*]						
31 (1)	10	5	40	20	15	10
32 (2)	30	10	15	0	20	25
33 (4)	20	10	10	35	15	10
34 (8)	45	20	5	5	20	5
35 (14)	0	0	20	55	10	15

[*] Numbers within brackets refer to the corresponding number of the sample without chlorite.

presence of quartz affects the scattering of light, thereby affecting the spectral features of the other minerals within the mixture. While the shape of the CR feature of a mineral is unlikely to be affected by quartz, the depth, asymmetry and saturation of the fitted Gaussians will likely be affected (Clark, 1999).

2.3.1.3. Selection of absorption components for curve fitting by EGO. Based on the number of minerals and their specific absorption behaviour, as discussed in the previous section, we expected that six individual absorption components centred around 2.170, 2.210, 2.250, 2.310, 2.350 and 2.380 μm would be required to optimally model abundances. From here on, these components are referred to as absorption components 1 to 6. For those spectra having 2 absorption features within the 2.100–2.400 μm region, the reflectance was split into the two primary absorption features around 2.120–2.270 μm and 2.280–2.400 μm, referred to as "feature 1" and "feature 2", respectively. Fig. 3 illustrates the positioning of the individual absorption components and features using the spectrum of pure kaolinite (Fig. 3).

2.3.2. Field experiment

2.3.2.1. Field sampling. The regional case study was located in Northern Morocco, centred at around 34.0° N, −4.5° W and covers an area of 15,000 km^2. While the Rif Mountains, an area of highlands, form the northern border, the Anti-Atlas Mountains is the southern border with areas of plateaus and intermountain valleys in between. This area offered a diverse lithological setting including sedimentary, igneous and metamorphic rock types. For training of the regression trees, a sample was collected which covered the variability in mineralogy present in the study area. We designed a sparse, remote sensing-based sampling approach making use of conditioned Latin Hypercube Sampling (cLHS) to assess variability in soil properties at regional scale (Mulder et al., 2012a).

At 73 sites, a mixed soil sample from a 15 × 15 m plot was taken of the top 5 cm of the soil. Two additional samples originating from a soil profile and duplicate samples of 2 sites were included which resulted in a total sample size of 77. The soil samples were dried at 70 °C, sieved and crushed to a powder (<20 μm) with a McCrone micronising mill in ethanol. To improve mineral quantification by X-ray diffraction, the organic matter was destroyed for samples having organic matter content higher than about 10%. Spectral measurements were taken with the same setup as described in Section 2.3.1 and the absorption components used for curve fitting and training of the regression tree were identical to those described in Section 2.3.1.

2.3.2.2. X-ray powder diffraction for analysis of soil mineralogical composition. Mineralogy of the fine powdered samples (<0.20 μm) was determined on randomly oriented powder specimens with X-ray diffraction analysis. The second sample preparation for clayey materials produces oriented specimens, which enhanced the basal reflections

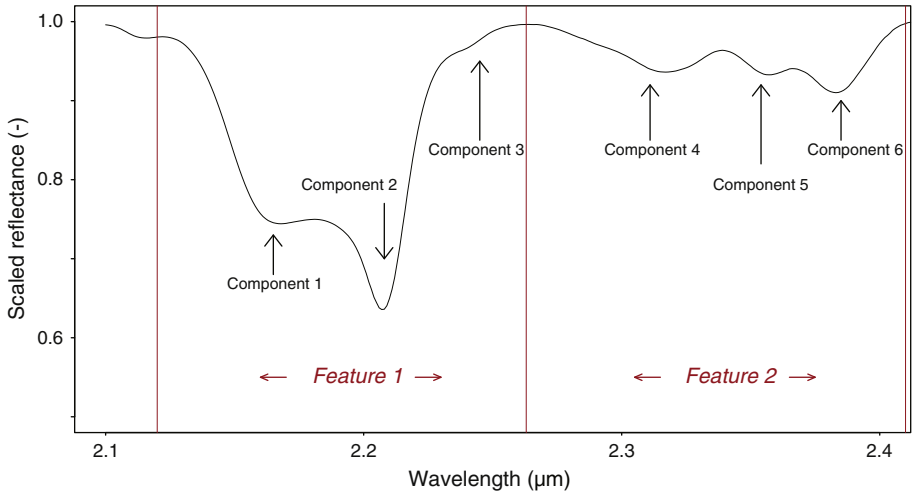

Fig. 3. Continuum removed spectrum of kaolinite where the absorption components within the 2.100–2.400 μm region are indicated along with the two spectral regions within the studied wavelength range (red lines).

Table 2
Ranges of the mineral abundance (wt.%) present in the field samples as determined by XRD analysis.

Mineral	Average (wt.%)	Range (wt.%)	Error (3σ) (wt.%)	No. samples
Anatase	1.0	0.4–1.9	0.2–0.3	41
Aragonite	7.1	1.9–11.1	0.7–0.8	3
Calcite	21.4	0.7–75.3	0.3–1.6	63
Chlorite	5.0	0.8–25.4	0.4–1.8	52
Cristobalite	2.8	1.2–4.5	0.3–0.5	3
Epidote	1.9	1.9	0.5	1
Dolomite	6.9	0.8–33.9	0.3–0.9	29
Goethite	5.2	1.2–11.6	0.8–1.3	14
Gypsum	1.5	1.5	0.5	1
Hematite	1.4	0.4–4.6	0.2–0.4	27
Dioctahedral mica	10.5	1.6–56.9	0.4–2.1	66
Kaolinite	6.7	1.3–16.7	1.1–2.7	49
K-feldspar	3.1	0.9–18.6	0.5–1.3	42
Palygorskite	6.8	6.8	0.8	1
Plagioclase Ab	4.9	1–23.8	0.4–1.2	69
Quartz	42.5	12.6–83.9	0.6–1.8	77
Rutile	1.1	0.6–1.8	0.2–0.4	10
Smectite	28.6	9.4–52.9	1.4–3.0	25
I/S ML	20.7	6.5–42.4	2.3–3.6	10

from the clay minerals thereby facilitating their identification. The changes in the reflex positions in the XRD pattern by intercalation of ethylene glycol were used for the identification of smectite. X-ray measurements were made using a Bragg–Brentano Theta–2Theta diffractometer Philips PW1820 using Cu Ka alpha radiation. The instrument was equipped with an automatic divergence slit, a graphite monochromator and a NaI scintillation counter. The powder samples were step-scanned at room temperature from 2 to 70° 2Theta (step width 0.03° 2Theta, counting time 4 s). The qualitative phase composition was determined in comparison to the Powder Diffraction File of the International Centre for Diffraction Data (ICDD PDF) database using the software DIFFRACplus (Bruker AXS, 2012). The quantitative mineral composition of the samples was calculated by Rietveld analysis using the Rietveld programme AutoQuan (GE SEIFERT) (Bergmann et al., 1998; Kleeberg, 2005).

The ranges and variety of minerals within the field samples, determined by XRD analysis, are presented in Table 2. Due to the similar structure of illite and muscovite, the minerals were not separated with the XRD analysis and are treated as the sum of dioctahedral mica in the field experiment. The interstratified illite/smectite minerals are summarised as I/S ML. This mineral type was not defined more in detail with respect to the ratio illite/smectite and order of layering. For the experiments those minerals were included which (1) had absorption features in the 2.100–2.400 μm region (Fig. 4), (2) were frequently present in the samples and (3) had an average content larger than 5%. Following these criteria, calcite, dioctahedral mica, smectite and kaolinite were considered in this study. The other minerals were deemed either subordinate to the selected minerals or did not contain the required spectral features to estimate abundances using spectral unmixing approaches.

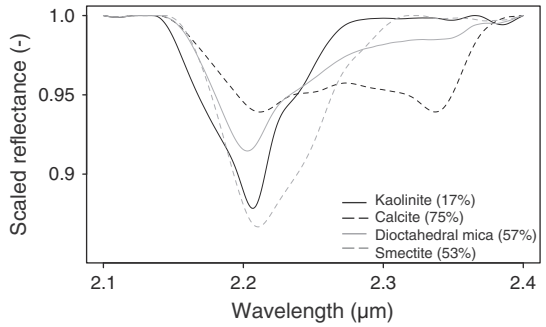

Fig. 4. Continuum removed spectra of the field samples with the highest individual abundances of kaolinite, calcite, dioctahedral mica and smectite.

The use of field samples may introduce several errors which could reduce the accuracy of the approach. The uncertainties are related to additional traces of other minerals and organic matter, significant amounts of minerals without diagnostic features in the 2.100–2.400 μm region and measurement errors. Also, differences in the accuracy of the XRD analysis might influence the prediction accuracy. As can be seen from Table 2, the error for the determined content of smectite (1.4–3.0 wt.%) and I/S ML (2.3–2.6 wt.%) was higher compared to the errors for calcite (0.3–1.6 wt.%), dioctahedral mica (0.4–2.1 wt.%) and kaolinite (1.1–2.7 wt.%). Note that the regression tree was trained only on the abundances of the minerals of interest. These minerals occur within an unknown matrix, which might interfere with the measurements and the subsequent analysis. However, owing to the sampling design we assume that the samples also represent the non-analysed minerals associated with the composition of interest. Although unknown constituents may affect the spectral behaviour this does not necessarily invalidate the approach since regression tree analysis can deal with non-linear behaviour and interactions. Training of the regression trees was done by using the XRD determined abundance of each mineral as the weight percentage of the mineral with respect to the total weight of the sample. Therefore, the regression tree predictions are also expressed as absolute weight percentages.

3. Results

3.1. Curve fitting

Table 3 shows the parameters of the EGO profiles fitted for the pure minerals; calcite was fitted with three EGO profiles positioned around the typical absorption components of calcite. The spectrum of calcite was fitted with one feature ranging from 2.120 to 2.400 μm. Dioctahedral mica required two EGO profiles positioned around the two strongest typical absorption components. The feature was split into two absorption features to obtain a better fit. Smectite was fitted with two EGO profiles positioned around the typical absorption features of smectite by one feature within 2.100–2.280 μm wavelength range. Kaolinite was fitted with four EGO profiles and was split into the wavelength ranges of 2.120–2.240 μm and 2.270–2.450 μm. The typical absorption between 2.120 and 2.240 μm was more difficult to fit by an EGO profile; this feature had the lowest fit of all the modelled features. Overall, the low values for the RMSE of the estimated log reflectance per feature show that the EGO profiles fitted on the typical absorption components of the mineral result in an accurate estimate of the measured log reflectance of the absorption features.

Table 4 provides the results of the deconvolution of the spectra from the 35 samples within the laboratory experiment. The total number of fitted profiles is given and the minimum and maximum parameter values as well. In addition, the average goodness of fit of all samples is provided by the average RMSE of the estimated log reflectance per feature for all 35 samples along with the standard deviation of the RMSE. The low average RMSE and standard deviation of the estimated log reflectance shows that the curve fitting approach approximates the measurements well. Splitting the reflectance into two spectral regions was necessary for most samples. The samples containing high concentrations of calcite were modelled by one feature. Samples containing relatively high concentrations of all four minerals required more EGO profiles compared to samples with specific dominant minerals to obtain the same accuracy.

The position of the EGO profiles corresponded to those of the diagnostic absorption features of the individual minerals, with minor shifts to smaller and longer wavelengths. In conclusion, the six expected absorption components of the minerals within the spectra were chosen to reflect their dimensionality. The minimum and maximum values of the saturation and asymmetry deviated strongly compared to the

Table 3
Model parameter values of the fitted EGO profiles to the pure minerals. In addition, the RMSE of the fitted log reflectance compared to the measured log reflectance is given for each mineral. The EGO profile numbers correspond to the absorption components as identified in Section 2.3.1.

	Calcite					**Dioctahedral mica**				
EGO Profile	Position	Intensity	Width	Saturation	Asymmetry	Position	Intensity	Width	Saturation	Asymmetry
1	2.158	0.012	0.010	–2.890	0.098	–	–	–	–	–
2	–	–	–	–	–	2.202	0.261	0.024	$-3.68 * 10^{-5}$	0.011
3	2.288	0.082	0.028	$-7.95 * 10^{-5}$	–0.356	–	–	–	–	–
4	–	–	–	–	–	–	–	–	–	–
5	2.338	–0.173	0.021	$1.10 * 10^{-4}$	–0.1000	2.341	0.050	0.014	–2.501	–0.111
6	–	–	–	–	–	–	–	–	–	–
		Feature1		Feature 2				Feature1		Feature 2
Continuum						Continuum				
	Offset	–5.165		–			Offset	–1.868		–4.723
	Slope	1.274		–			Slope	3.456		–9.971
RMSE		0.0008		–		RMSE		0.0035		0.0011

	Smectite					**Kaolinite**				
EGO Profile	Position	Intensity	Width	Saturation	Asymmetry	Position	Intensity	Width	Saturation	Asymmetry
1	–	–	–	–	–	2.164	–0.360	0.025	$-2.87 * 10^{-4}$	–0.326
2	2.205	0.196	0.018	0.920	–0.073	2.206	0.0446	0.011	$-1.48 * 10^{-5}$	–0.147
3	2.239	0.062	0.010	0.883	0.101	–	–	–	–	–
4	–	–	–	–	–	–	–	–	–	–
5	–	–	–	–	–	2.357	0.035	$6.20 * 10^{-3}$	2.097	0.055
6	–	–	–	–	–	2.384	0.076	$9.82 * 10^{-3}$	0.355	–0.012
		Feature1		Feature 2				Feature1		Feature 2
Continuum						Continuum				
	Offset	–1.563		–			Offset	–8.329		–3.27
	Slope	3.091		–			Slope	17.590		6.27
RMSE		0.0016		–		RMSE		0.0166		0.0014

Each absorption component is described by a position (μm), width as the full width at half maximum (μm), intensity (μm), saturation (−) and asymmetry (−). The values listed for each continuum are the offset and slope of a straight line in wavelength and natural log reflectance.

values of the EGO profiles fitted to the pure minerals, especially for the profiles 1, 3, 5 and 6. This indicates that the central limit theorem does not fully apply to the spectra of mineral mixtures. To accurately fit the absorption around the defined components, the EGO profile is required to be modelled with use of the parameters for asymmetry and saturation.

Table 5 provides the results of the deconvolution of the spectra from the 77 samples within the field experiment. In addition, the average goodness of fit of all samples is provided by the average RMSE of the estimated log reflectance per feature for all 77 samples along with the standard deviation of the RMSE. The average RMSE and its standard deviation of the estimated log reflectance show that the curve fitting resulted in small differences between the observed and predicted log reflectance. Of most interest are the differences between the obtained parameter values compared to those of the laboratory experiment. The field samples required fewer EGO profiles than the laboratory experiment which can be attributed to the fact that most of these samples consisted of at most two dominant minerals. The intensities were lower and the saturation and asymmetry effects strongly increased. The shifts in position towards higher and lower wavelengths were also stronger but they were still well modelled by the six absorption components of the minerals. Fewer

Table 4
Model parameters of the EGO profiles fitted to the 35 prepared samples. For each EGO profile the total number of fitted profiles and the minimum and maximum parameters values are given. In addition, the average RMSE and standard deviation of the fitted log reflectance for the full sample is given.

EGO profile	No. of samples	Position		Intensity		Width		Saturation		Asymmetry	
		Min	Max	Min	Max	Min	Max	Min	Max	Min	Max
1	24	2.158	2.193	–0.360	0.134	0.009	0.025	–4.842	38.88	–0.327	0.098
2	32	2.201	2.208	0.005	0.446	0.011	0.024	–0.501	0.920	–0.260	0.221
3	24	2.216	2.253	–0.069	0.100	–0.013	0.018	–3.343	14.57	–0.226	0.199
4	10	2.284	2.309	–0.057	0.082	0.008	0.032	–3.987	3.705	–0.427	0.027
5	27	2.337	2.357	–0.173	0.077	0.006	0.022	–44.87	13.61	–0.305	0.055
6	14	2.364	2.385	0.006	0.076	0.006	0.015	–30.50	6.107	–0.438	0.093
		Feature1						Feature 2			
		Average	Standard deviation					Average	Standard deviation		
RMSE		0.00189	0.0028					0.00058	0.00030		

Each absorption component is described an EGO profile which has a position (μm), width as the full width at half maximum (μm), intensity (μm), saturation (−) and asymmetry (−). The RMSE provides the measure for goodness of fit of the estimated log reflectance compared to the measured log reflectance of the prepared samples.

Table 5
Model parameters of the EGO profiles fitted to the 77 field samples. For each EGO profile the total number of fitted profiles and the minimum and maximum parameters values are given. In addition, the average RMSE and standard deviation of the fitted log reflectance for the full sample is given.

EGO profile	No. fitted	Position		Intensity		Width		Saturation		Asymmetry	
		Min	Max	Min	Max	Min	Max	Min	Max	Min	Max
1	37	2.171	2.198	0.008	0.078	0.008	0.028	–6.824	8.253	–0.165	0.110
2	75	2.202	2.216	–0.077	0.165	0.007	0.028	–9.114	1.136	–0.217	0.266
3	72	2.215	2.333	–0.026	0.062	0.008	0.019	–4.953	48.96	–0.160	0.300
4	13	2.281	2.309	–0.017	0.041	–0.009	0.035	–11.81	14.15	–0.445	0.290
5	65	2.312	2.369	–0.014	0.064	0.006	0.187	–21.98	56.68	–1.016	1.692
6	9	2.376	2.396	–0.013	0.015	0.005	0.505	–6.863	11.14	–0.307	3.618

	Feature1		Feature 2	
	Average	Standard deviation	Average	Standard deviation
RMSE	0.0020	0.0006	0.00056	0.00034

Each absorption component is described by a position (μm), a full width at half maximum (μm), intensity (μm), saturation (—) and asymmetry (—). The RMSE provides the measure of goodness of fit of the predicted log reflectance compared to the observed log reflectance of the field samples.

EGOs were fitted around the smaller absorption components (1, 4 and 6) which could indicate that the weaker absorption components of the minerals, around 2.170 μm, 2.310 μm and 2.380 μm, became subsidiary absorptions. Overall, the appearances of individual absorption components were less intense in the field samples due to the noise introduced relating to the additional traces of other minerals, significant concentrations of minerals without diagnostic features in the 2.100–2.400 μm region (Table 2).

3.2. Prediction of mineralogy by regression trees

3.2.1. Laboratory experiment

The mineral abundances of the prepared samples were predicted by pruned regression trees which included a maximum of seven EGO variables (Table 6). The splits of the regression trees were mainly based on the position, intensity and width of the EGO profiles. The predicted samples fell into the numerical ranges defined by the terminal nodes of the regression tree. For example, Fig. 5 shows the pruned regression tree for dioctahedral mica where the variables with the threshold to split the dataset are given at the nodes and the total number of samples assigned to each terminal node.

Cross-validation of the pruned regression trees shows that (Fig. 6a–d); kaolinite resulted in six terminal nodes and abundance was predicted with a RMSE of 4 wt.% and R^2 of 0.92. Dioctahedral mica resulted in eight terminal nodes and was predicted by the regression tree with an RMSE of 9.3 wt.% and R^2 of 0.82. Calcite resulted in eight terminal nodes and was predicted by the regression tree with an RMSE of 7.3 wt.% and R^2 of 0.88. Smectite resulted in seven terminal nodes and was predicted by the regression tree with an RMSE of 8 wt.% and R^2 of 0.85. Calculation of the covariance of the predicted minus the measured mineral abundance showed that neither the over- or under estimation of a mineral were correlated to the other minerals.

Table 6
Variables used at splits in the pruned regression trees for the laboratory experiment.

Regression tree	EGO profile parameters				
	Position	Intensity	Width	Asymmetry	Saturation
Kaolinite		EGO 2*	EGO 1		
		EGO 3	EGO 2		
			EGO 3		
Dioctahedral mica	EGO 3	EGO 3	EGO 2	EGO 2	EGO 2
		EGO 5			EGO 5
Smectite	EGO 3	EGO 1	EGO 2	EGO 2	EGO 2
Calcite	EGO 1	EGO 2	EGO 2	EGO 1	
			EGO 5		

* EGO 1: 2.170 μm, EGO 2: 2.210 μm, EGO 3: 2.250 μm and EGO 5: 2.350 μm.

For dioctahedral mica the major splits in the regression tree were based on the position and intensity of the absorption component around 2.250 μm, and the width, asymmetry and saturation around 2.210 μm. Smaller splits used the intensity and saturation around 2.350 μm (Table 6). The major splits for the pruned regression tree for kaolinite were based on the intensity and width of the EGO profiles around 2.210 μm and 2.250 μm and smaller splits used the width around 2.170 μm (Table 6). Although the small subsidiary absorptions at wavelengths of >2.250 μm could be fitted, they were not significantly present within the mixture to be used as a prediction parameter. The EGO profiles corresponding to the typical absorption components of smectite around 2.210 μm and 2.250 μm were used for partitioning of the dataset; the asymmetry and saturation of the EGO profile around 2.210 μm and the position around 2.250 μm were used for the major splits. The typical v-shape of the smectite absorption becomes less distinct and intense within mixtures due to saturation. With increasing saturation of the absorption component around 2.250 μm the width of the EGO profile around 2.210 μm and the asymmetry of the EGO profile around 2.250 μm increases. The prediction of calcite was based on the width of the EGO profile around 2.350 μm, and the position around 2.170 μm and the parameters related to the EGO profile around 2.210 μm. Taking into account the strong absorption components of calcite around 2.350 μm (Fig. 2), it was to be expected that changes related to this feature would be important for defining the splits of the regression tree.

In Table 7 the differences between the predicted mineralogy from the samples with added chlorite are given. Small errors occur up to 3 wt.%, with the exception of smectite in sample 2 and dioctahedral mica in sample 14, and the latter deviating just 6 wt.% difference with the measured content. Mineral concentrations in most of these "contaminated" samples

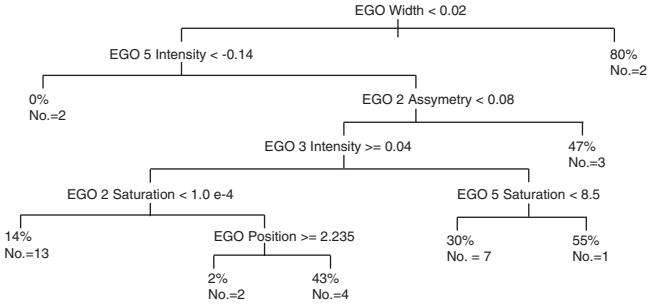

Fig. 5. Regression tree for dioctahedral mica, the thresholds at a specific split with the assigned EGO parameter, the mineral abundance (wt.%) and the number of samples for each terminal node are given.

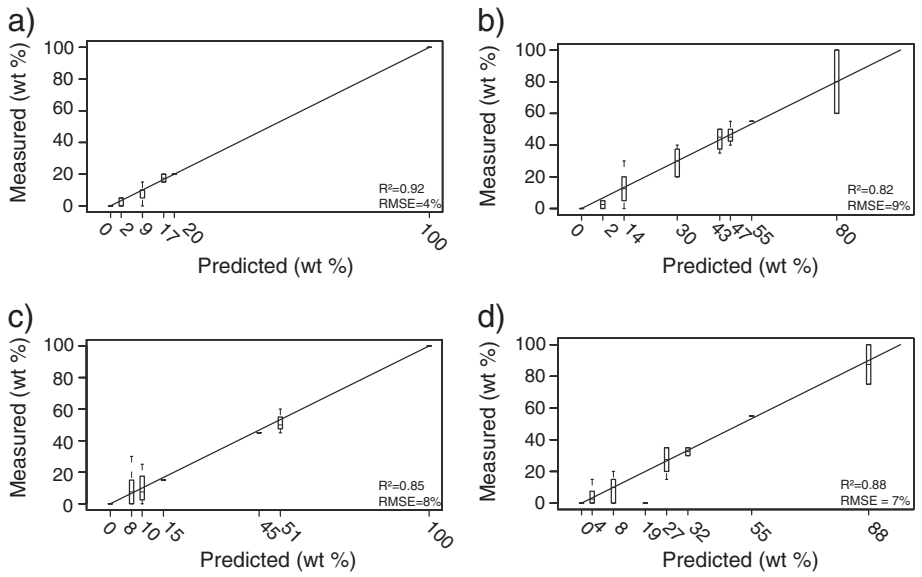

Fig. 6. a–d. Predicted relative mineral content (wt.%) from the laboratory experiment compared to known mineral abundance for a) kaolinite, b) mica, c) smectite and d) calcite. The predicted mineralogy is presented by boxplots of the samples which were assigned to the terminal nodes of the regression tree.

were predicted correctly. This indicates that the pruned regression trees trained on the specific mineral absorption components were rather insensitive to contamination by chlorite.

Finally, the absorption components around 2.210 μm and 2.350 μm were most diagnostic; modelled changes of these components and their relation to the other components were the key to predicting mineralogy in composite mixtures. These results and the constructed regression trees show that indeed there is a statistical relationship between the model parameters and their representativeness of the complex interaction between diagnostic absorptions and mineralogy. Although intensity and widening were the most important parameters, some regression trees required the parameters related to saturation or asymmetry which stresses the added value of including these parameters for the deconvolution of the spectra. Note that our sample was small, which resulted in simple trees with few terminal nodes; a larger sample of mineral mixtures spanning the volume space may produce more complex trees with finer resolution in the terminal nodes.

Table 7
Difference in the predicted mineralogy of the samples containing additional chlorite.

Sample no.	Mineral	Content (%)	Predicted content (%)		Difference between predicted contents
			Original sample	Sample with chlorite	
1	Kaolinite	5	8.9	8.9	0.0
	Dioctahedral mica	40	29.3	29.3	0.0
	Smectite	10	8.5	8.5	0.0
	Calcite	20	27.5	27.5	0.0
2	Kaolinite	15	8.9	8.9	0.0
	Dioctahedral mica	15	13.9	13.9	0.0
	Smectite	45	51.3	8.5	−42.7
	Calcite	0	4.4	0.0	−4.4
4	Kaolinite	10	8.9	8.9	0.0
	Dioctahedral mica	10	13.9	13.9	0.0
	Smectite	20	10.0	8.5	−1.5
	Calcite	35	27.5	27.5	0.0
8	Kaolinite	20	17.5	17.5	0.0
	Dioctahedral mica	5	13.9	13.9	0.0
	Smectite	45	45.0	45.0	0.0
	Calcite	5	4.4	8.3	3.9
14	Kaolinite	0	2.1	2.1	0.0
	Dioctahedral mica	20	29.3	13.9	−15.4
	Smectite	0	8.5	8.5	0.0
	Calcite	55	55.0	55.0	0.0

3.2.2. Field experiment

The relative mineral abundance in the field samples was predicted by training and pruning the regression trees by the same EGO profiles used for the laboratory experiment. New regression trees were trained because unknown constituents may have affected the spectral behaviour and thereby changing the relation of the EGO parameters and mineral abundances. The regression trees included a maximum of five variables for their splits (Table 8). The coefficient of determination (R^2) and RMSE of predicted mineral content (wt.%) obtained from cross validation of the pruned regression trees generally were lower compared to the controlled experiments. This indicates that the fit of the trees were less accurate and the estimated error in the mineral abundance was consequently lower. Because more samples were available for training of the tree, more terminal nodes could be made and thereby the error estimate of the mineral abundance reduced. The splits of the regression trees were mainly based on intensity and asymmetry rather than the position, intensity and width of the trees in the laboratory experiment. Kaolinite

Table 8
Variables used at splits in the pruned regression trees for the field experiment.

Regression tree	EGO parameter values				
	Position	Intensity	Width	Asymmetry	Saturation
Kaolinite	EGO 3*		EGO 2	EGO 2 EGO 3	
Dioctahedral mica		EGO 2 EGO 5		EGO 2 EGO 3	EGO 2
Smectite		EGO 2 EGO 3		EGO 2 EGO 3	
Calcite	EGO 5	EGO 5		EGO 1 EGO 2	

* EGO 1: 2.170 μm, EGO 2: 2.210 μm, EGO 3: 2.250 μm and EGO 5: 2.350 μm.

resulted in seven terminal nodes and abundance was predicted with an RMSE of 3 wt.% and R^2 of 0.70 (Fig. 7a). The deviations occur in samples where absence was predicted while the actual content of the samples where within a range of 0–8 wt.% kaolinite. Dioctahedral mica resulted in eight terminal nodes and was predicted by the regression tree with an RMSE 5 wt.% and R^2 of 0.63 (Fig. 7b). Calcite resulted in seven terminal nodes and was predicted by the regression tree with an RMSE 8 wt.% and R^2 of 0.80 (Fig. 7d). The nodes including the absence and traces of calcite contained the samples with the greatest deviation resulting in a general underestimation of calcite. Unfortunately, with respect to smectite it was not possible to build a regression tree with a better fit and accuracy ($R^2 = 0.40$, RMSE = 12 wt.%) (Fig. 7c) without violating the criteria set for pruning the regression tree. Calculation of the covariance of the predicted minus the measured mineral abundance showed that neither the over- or under estimation of a mineral were correlated to the other minerals.

The independent validation on 16 samples resulted in an RMSE of 5 wt.% for kaolinite, 9 wt.% for dioctahedral mica, 18 wt.% for smectite and 14 wt.% for calcite. The overall lower RMSE (%) within the field experiment can be attributed to specific mineral composition of the field samples compared to the prepared samples. The relative abundance of minerals was usually dominated by two minerals with only smaller contributions of other minerals. Also, more samples were available for training the regression tree. From Fig. 7(a–d) it can also be observed that the model has difficulties with the prediction of the absence of minerals; the main reason can be attributed to the precision of the tree, due to the small sample (smectite, the smallest set consisted of 25 samples) few terminal nodes could be set. For both kaolinite and dioctahedral mica the model estimates a presence up to 5 wt.% in samples where these minerals are absent. For calcite and smectite the abundance estimate for absent minerals is up to a maximum of 10 wt.%. These lower thresholds for kaolinite and dioctahedral mica can be attributed to lower abundance in the samples used for training the trees.

4. Discussion

This work demonstrated that the combination of spectral deconvolution of SWIR spectra with regression tree analysis allows simultaneous quantification of more than two minerals within a mixture. The fact that more than two minerals can be simultaneously quantified is an improvement on similar MGM based methods. Key to this improvement was the regression tree analysis that followed the EGO analysis.

It was found that the degree of expression of absorption components was different between the field samples and the laboratory mixtures. Due to the nature of the field samples, the simple representation of the complex scattering behaviour by a few Gaussian bands required asymmetry and saturation to accurately deconvolve the spectra. Also, asymmetry of the EGO profiles proved to be an important parameter for the estimation of mineral content with field samples. For operational use, these results emphasise the importance of using (1) field samples for training of the model rather than laboratory mixes and (2) deconvolution using the EGO algorithm. For terrestrial studies it is therefore recommended that a representative surface sample is collected using a strategic sampling design, such as the one used by Mulder et al. (2012a).

The regression tree analysis was an improvement on the band ratios (Kanner et al., 2007; Noble et al., 2006) and the multiple linear regression (MLR) (Bishop et al., 2011) that were used to relate mineral abundances to the parameterised reflectance of mineral mixtures. Regression trees can deal with nonlinearity and interactions between the EGO parameters which made it possible to accurately predict mineral abundances from complex mixtures. The regression tree analysis used in this work uses a heuristic approach of making local optimal choices and finding a global optimum (cf., greedy algorithm), whereby construction of the tree is based on a local optimisation, that is at each node the data are partitioned — giving the best result for that specific node. This local optimisation can result in an initial split based on some criteria which at subsequent levels result in suboptimal splits. Improvements are expected by using less greedy algorithms such as boosted regression trees or random forest (Brown et al., 2006).

Alternatively, methods based on the single scattering albedo model of Hapke (Hapke, 2002), such as the work of Warell and Davidsson (2010) and Mustard and Pieters (1987), have proven successful in simultaneous retrieval of mineral abundances from prepared mixtures. Despite that, the accuracy of estimated mineral abundances from natural samples proved to be rather low. Our method is a strong competitor of the Hapke-based models. Especially, considering the required detailed information on the scattering properties of all endmembers in the model of Hapke (Keshava and Mustard, 2002) and the lower accuracy for estimates from natural samples (Warell and Davidsson, 2010). Nevertheless, there are limitations to our approach and possible solutions as outlined below.

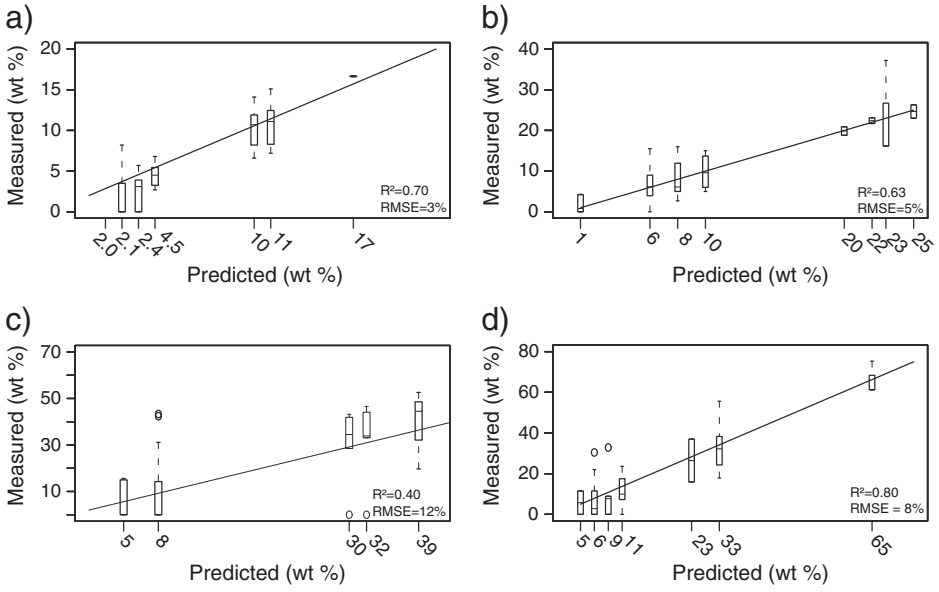

Fig. 7. a–d. Predicted relative mineral content (wt.%) from the field experiment compared to the values obtained from the XRD analysis for a) kaolinite, b) mica, c) smectite and d) calcite. The predicted mineralogy is presented by boxplots of the samples which were assigned to the terminal nodes of the regression tree.

4.1. Limitations and outlook

4.1.1. Retrieval of smectite abundances

A likely explanation for the unsuccessful prediction of smectite is that smectite is a group consisting of monoclinic clay minerals such as e.g. montmorillonite. Within this group the clays have different ions within the octahedral layer; particularly Fe^{3+}or Al^{3+}, but also Mg^{2+}, occur depending on the dioctahedral or trioctahedral character of the octahedral layer (Moore and Reynolds, 1997). Mg is not commonly present in a dioctahedral layer but can be present due to charge compensation in the tetrahedral layers. Within the studied wavelength range strong absorption features of minerals are related to the overtones and combinations of the fundamentals of either the OH bend of AlOH, MgOH or Fe^{3+}OH. Also, within the laboratory experiment Na-rich montmorillonite was used, while the field samples originate from a calcite-rich environment resulting in Ca-rich montmorillonite. As discussed by Clark et al. (1990), variations in the Na/Ca ratio cause shifts of the 2.200 μm feature and with increasing Ca^{2+} concentrations the 2.250 μm feature becomes less pronounced (see also Figs. 2 and 4). The prediction model for smectite was trained by using both absorptions, which subsequently resulted in poor performance. As indicated by Bishop et al. (2011); if differences in the octahedral cations occur, samples should not be treated spectrally as one group (Bishop et al., 2011). So, by discriminating among the dioctahedral clay minerals by their variations in their cation concentrations and by training the regression trees individually, the prediction of smectite abundance could be improved.

4.1.2. Outlook

A contribution that could not yet be included is abundance estimates from other minerals having their absorption features outside the studied wavelength range. Common minerals found on Earth, besides quartz and feldspars e.g. goethite, hematite or chlorite, have their electronic absorption bands at shorter wavelengths. Similar, dominant soil minerals such quartz, alkali feldspars and plagioclases have fundamental absorptions in the MIR and occasionally have broad electronic absorption around 1.2 μm due to structural Fe. Within the domain of reflectance spectroscopy it would be recommended to extend the studied wavelength range to the full VNIR–SWIR range (0.4–3.0 μm) to allow analyses of more minerals which is feasible since most spectrometers usually cover this wavelength range.

Another challenge for the future includes the integration of the suggested approach with a spatial component. Spatially explicit information provides important information on parent material and soil formation (Egli et al., 2008; Mavris et al., 2011). Currently, satellites do not provide the fine spectral resolution needed to accurately deconvolve the spectra into components that can be related to mineral abundances. As a result, recent research efforts especially focus on the exploration and identification of minerals rather than abundances using RS data (Lau et al., 2012; Sgavetti et al., 2009; van der Meer et al., 2012; Viscarra Rossel, 2011). Compared to our work these studies do have a spatial context and provide insight in the spatial distribution of mineral characterisation within a study area. However, combining the presented work with additional geostatistical analysis could be key to e.g. the creation of mineral abundance maps of large areas.

5. Conclusions

The retrieval of mineralogy from SWIR reflectance presented and evaluated in this paper aims to estimate the modal abundance of multiple minerals by a spectral curve fitting approach. Subsequently, the model parameters were used to predict mineral abundance by regression tree analysis. By using EGO, the spectra between 2.100 μm and 2.400 μm were accurately fitted in both the laboratory and field experiment (average RMSE of 0.004). This required the isolation of the absorption features and modelling of the individual absorption components within these absorption complexes. The position of the absorption components compared to those of the known diagnostic absorption features of the individual minerals showed shifts towards shorter and longer wavelengths. The parameters addressing the saturation and asymmetry of the absorption components appeared to be essential to obtain an accurate fit for the field samples.

The regression trees calibrated for the laboratory experiment based the splits mainly on the position, intensity and width of the fitted absorption components. The calibrated trees in the field experiment resulted in splits based on intensity and asymmetry rather than position, intensity and width. The selected parameters reflected the major changes in absorption of specific minerals and to changes in relation to the other known minerals.

The cross-validation results showed that the regression tree models were able to predict the mineral abundances well by establishing the statistical relationship with the EGO model parameters. Within the laboratory experiment abundance of kaolinite, dioctahedral mica, calcite and smectite were predicted with respectable RMSE values of less than 9 wt.% and a minimum detection limit up to 10 wt.%. Prediction of mineralogy with field samples showed good results for calcite, dioctahedral mica and kaolinite, with RMSE values less than 8 wt.%, similar minimum detection limits but lower coefficients of determination. Prediction of smectite abundance was less successful due to the spectral variations related to differences in the octahedral cations in the smectites of the analysed powders. Substitution of part of the quartz by chlorite at the prediction phase hardly affected the accuracy of the predicted mineral contents; this suggests that the method is robust in handling the omission of minerals during the training phase. On the other hand, the degree of expression of absorption components was different between the field samples and the laboratory mixtures. This demonstrates that the method should be calibrated and trained on a training set representing the range of local mineral compositions. With this study we demonstrated that our method allows estimation of more than two minerals within a mixture and thereby enhances the perspectives of spectral analysis for mineral abundances.

Acknowledgements

We acknowledge financial support from the EU FP7 programme under the e-SOTER project (contract 211578). This study benefitted greatly from the review by G.A. Swayze and other anonymous reviewers. We thank H. Bartholomeus for his useful comments and L. Pompilio for making available the EGO algorithm and her insightful comments. R. Kokaly was supported by the Climate and Land Use Change Research & Development Program of the U.S. Geological Survey. We applied the SDC approach for the sequence of authors (Tscharntke et al., 2007).

Disclaimer

Any use of trade, firm, or product names is for descriptive purposes only and does not imply endorsement by the U.S. Government.

References

Ben-Dor, E., Chabrillat, S., Demattê, J.A.M., Taylor, G.R., Hill, J., Whiting, M.L., Sommer, S., 2009. Using imaging spectroscopy to study soil properties. Remote Sensing of Environment 113 (Suppl. 1), S38–S55.

Bergmann, J., Friedel, P., Kleeberg, R., 1998. BGMN — a new fundamental parameters based Rietveld program for laboratory X-ray sources, it's use in quantitative analysis and structure investigations, CPD Newsletter. Commission of Powder Diffraction, International Union of Crystallography. 5–8.

Bish, D.L., Plötze, M., 2011. X-ray powder diffraction with emphasis on qualitative and quantitative analysis in industrial mineralogy. In: Christidis, G. (Ed.), Industrial Mineralogy, EMU Notes in Mineralogy, pp. 35–76.

Bishop, J.L., Gates, W.P., Makarewicz, H.D., McKeown, N.K., Hiroi, T., 2011. Reflectance spectroscopy of beidellites and their importance for Mars. Clays and Clay Minerals 59 (4), 378–399.

Breiman, L., Friedman, J.H., Olshen, R.A., Sonte, C.J., 1984. Classification and Regression Trees. Wadsworth International Group, Belmont, California.

Brown, D.J., Shepherd, K.D., Walsh, M.G., Dewayne Mays, M., Reinsch, T.G., 2006. Global soil characterization with VNIR diffuse reflectance spectroscopy. Geoderma 132 (3–4), 273–290.
Bruker AXS, 2012. DIFFRACplus Software Solutions for X-ray Powder Diffraction.
Burns, R.G., 1993. Mineralogical Applications of Crystal Field Theory. Cambridge University Press.
Clark, R.N., 1998. Material absorption band depth mapping of imaging spectrometer data using a complete band shape least-squares fit with library reference spectra. U.S. Geological Survey, Denver, p. 11.
Clark, R.N., 1999. Chapter 1: Spectroscopy of Rocks and Minerals, and Principles of Spectroscopy.
Clark, R.N., King, T.V.V., Klejwa, M., Swayze, G.A., Vergo, N., 1990. High spectral resolution reflectance spectroscopy of minerals. Journal of Geophysical Research 95 (B8), 12653–12680.
Clark, R.N., Swayze, G.A., Livo, K.E., Kokaly, R.F., Sutley, S.J., Dalton, J.B., McDougal, R.R., Gent, C.A., 2003. Imaging spectroscopy: earth and planetary remote sensing with the USGS Tetracorder and expert systems. Journal of Geophysical Research 108 (E12), 5131.
Clénet, H., Pinet, P., Daydou, Y., Heuripeau, F., Rosemberg, C., Baratoux, D., Chevrel, S., 2011. A new systematic approach using the Modified Gaussian Model: insight for the characterization of chemical composition of olivines, pyroxenes and olivine–pyroxene mixtures. Icarus 213 (1), 404–422.
Dalton, J.B., Bove, D.J., Mladinich, C.S., Rockwell, B.W., 2004. Identification of spectrally similar materials using the USGS Tetracorder algorithm: the calcite–epidote–chlorite problem. Remote Sensing of Environment 89 (4), 455–466.
De'Ath, G., Fabricius, K.E., 2000. Classification and regression trees: a powerful yet simple technique for ecological data analysis. Ecology 81 (11), 3178–3192.
Dennison, P.E., Roberts, D.A., 2003. Endmember selection for multiple endmember spectral mixture analysis using endmember average RMSE. Remote Sensing of Environment 87 (2–3), 123–135.
Egli, M., Nater, M., Mirabella, A., Raimondi, S., Plötze, M., Alioth, L., 2008. Clay minerals, oxyhydroxide formation, element leaching and humus development in volcanic soils. Geoderma 143 (1–2), 101–114.
Flahaut, J., Quantin, C., Clenet, H., Allemand, P., Mustard, J.F., Thomas, P., 2012. Pristine Noachian crust and key geologic transitions in the lower walls of Valles Marineris: insights into early igneous processes on Mars. Icarus 221 (1), 420–435.
Garbow, B.S., Hillstrom, K.E., More, J.J., 1980. MINPACK project. http://www.netlib.org/minpack/.
Gomez, C., Lagacherie, P., Coulouma, G., 2008. Continuum removal versus PLSR method for clay and calcium carbonate content estimation from laboratory and airborne hyperspectral measurements. Geoderma 148 (2), 141–148.
Hapke, B., 2002. Bidirectional reflectance spectroscopy. 5. The coherent backscatter opposition effect and anisotropic scattering. Icarus 157 (2), 523–534.
Hong, H., Li, Z., Xue, H., Zhu, Y., Zhang, K., Xiang, S., 2007. Oligocene clay mineralogy of the Linxia Basin: evidence of Paleoclimatic evolution subsequent to the initial-stage uplift of the Tibetan Plateau. Clays and Clay Minerals 55 (5), 491–503.
Kanner, L.C., Mustard, J.F., Gendrin, A., 2007. Assessing the limits of the Modified Gaussian Model for remote spectroscopic studies of pyroxenes on Mars. Icarus 187 (2), 442–456.
Keshava, N., Mustard, J.F., 2002. Spectral unmixing. IEEE Signal Processing Magazine 19 (1), 44–57. http://dx.doi.org/10.1109/79.974727.
Kleeberg, R., 2005. Results of the second Reynolds Cup contest in quantitative mineral analysis. CPD Newsletter 30, 3.
Lane, M.D., Glotch, T.D., Dyar, M.D., Pieters, C.M., Klima, R., Hiroi, T., Bishop, J.L., Sunshine, J., 2011. Midinfrared spectroscopy of synthetic olivines: thermal emission, specular and diffuse reflectance, and attenuated total reflectance studies of forsterite to fayalite. Journal of Geophysical Research 116 (E8), E08010.
Lau, I.C., Cudahy, T.J., Caccetta, M.C., Kobayashi, C., Kashimura, O., Kato, M., Wheaton, G.A., Carter, D.J., 2012. Mapping surface soil mineralogy using hyperspectral and ASTER imagery: An example from Mullewa, Western Australia, Digital Soil Assessments and Beyond — Proceedings of the Fifth Global Workshop on Digital Soil Mapping, pp. 365–371.
Mavris, C., Plötze, M., Mirabella, A., Giaccai, D., Valboa, G., Egli, M., 2011. Clay mineral evolution along a soil chronosequence in an Alpine proglacial area. Geoderma 165 (1), 106–117.
McBratney, A.B., Santos, M.L., Minasny, B., 2003. On digital soil mapping. Geoderma 117 (1–2), 3–52.
Moore, D.M., Reynolds Jr., R.C., 1997. Diffraction and the Identification and Analysis of Clay Minerals, 2nd ed. Oxford University Press, New York.
Moré, J.J., 1978. The Levenberg–Marquardt algorithm: implementation and theory. Lecture Notes in Mathematics 630.Springer-Verlag, New-York.
Mulder, V.L., de Bruin, S., Schaepman, M.E., Mayr, T.R., 2011. The use of remote sensing in soil and terrain mapping — a review. Geoderma 162 (1–2), 1–19.
Mulder, V.L., de Bruin, S., Schaepman, M.E., 2012a. Representing major soil variability at regional scale by constrained Latin Hypercube Sampling of remote sensing data. International Journal of Applied Earth Observation and Geoinformation 21 (1), 301–310.
Mulder, V.L., de Bruin, S., Schaepman, M.E., 2012b. Retrieval of composite mineralogy by VNIR spectroscopy. In: Minasny, B. (Ed.), Digital Soil Assessments and Beyond: Proceedings of the 5th Global Workshop on Digital Soil Mapping 2012. CRC Press, Sydney, Australia, p. 488.
Mustard, J.F., Pieters, C.M., 1987. Quantitative abundance estimates from bidirectional reflectance measurements. Journal of Geophysical Research: Solid Earth 92, E617–E626.
Noble, S.K., Pieters, C.M., Hiroi, T., Taylor, L.A., 2006. Using the modified Gaussian model to extract quantitative data from lunar soils. Journal of Geophysical Research E: Planets 111.
Ogawa, Y., Matsunaga, T., Nakamura, R., Saiki, K., Ohtake, M., Hiroi, T., Takeda, H., Arai, T., Yokota, Y., Yamamoto, S., Hirata, N., Sugihara, T., Sasaki, S., Haruyama, J., Morota, T., Honda, C., Demura, H., Kitazato, K., Terazono, J., Asada, N., 2011. The widespread occurrence of high-calcium pyroxene in bright-ray craters on the Moon and implications for lunar-crust composition. Geophysical Research Letters 38 (17), L17202.
Omotoso, O., McCarty, D.K., Hillier, S., Kleeberg, R., 2006. Some successful approaches to quantitative mineral analysis as revealed by the 3rd Reynolds Cup contest. Clays and Clay Minerals 54 (6), 748–760.
Pinet, P.C.H.F., Clenet, H., Chevrel, S., Daydou, Y., Baratoux, D., Rosemberg, C., Bibring, J.P., Poulet, F., Gondet, B., Mustard, J., Le Mouélic, S., Bellucci, G., OMEGA Team, 2007. Mafic mineralogy variations across syrtis major shield and surroundings as inferred from visible-near-infrared spectroscopy by OMEGA/Mars Express. Seventh International Conference on Mars, Pasadena, California, p. 3146.
Pompilio, L., Pedrazzi, G., Sgavetti, M., Cloutis, E.A., Craig, M.A., Roush, T.L., 2009. Exponential Gaussian approach for spectral modeling: the EGO algorithm I. Band saturation. Icarus 201 (2), 781–794.
Pompilio, L., Pedrazzi, G., Cloutis, E.A., Craig, M.A., Roush, T.L., 2010. Exponential Gaussian approach for spectral modelling: the EGO algorithm II. Band asymmetry. Icarus 208 (2), 811–823.
Press, W.H., Flannery, B.P., Teukolsky, S.A., Vetterling, W.T., 1992. Numerical Recipes in FORTRAN: The Art of Scientific Computing, 2nd ed. Cambridge University Press, Cambridge.
R Development Core Team, 2011. R: A Language and Environment for Statistical Computing. R Foundation for Statistical Computing, Vienna, Austria.
Ripley, B., 2011. Recursive Partitioning. R Package version 3.1–50. (http://CRAN.R-project.org/package=rpart).
Roush, T.L., Singer, R.B., 1986. Gaussian analysis of temperature effects on the reflectance spectra of mafic minerals in the 1 μm region. Journal of Geophysical Research 91 (B10), 10301–10308.
Sassaroli, A., Fantini, S., 2004. Comment on the modified Beer–Lambert law for scattering media. Physics in Medicine and Biology 49 (14), 3.
Sedov, S., Solleiro-Rebolledo, E., Morales-Puente, P., Arias-Herreìa, A., Vallejo-Gèomez, E., Jasso-Castaneda, C., 2003. Mineral and organic components of the buried paleosols of the Nevado de Toluca, Central Mexico as indicators of paleoenvironments and soil evolution. Quaternary International 106–107, 169–184.
Sgavetti, M., Pompilio, L., Roveri, M., Manzi, V., Valentino, G.M., Lugli, S., Carli, C., Amici, S., Marchese, F., Lacava, T., 2009. Two geologic systems providing terrestrial analogues for the exploration of sulfate deposits on Mars: initial spectral characterization. Planetary and Space Science 57 (5–6), 614–627.
Shepard, M.K., Helfenstein, P., 2007. A test of the Hapke photometric model. Journal of Geophysical Research 112 (E3), E03001.
Singer, R.B., 1981. Near-infrared spectral reflectance of mineral mixtures: systematic combinations of pyroxenes, olives, and iron oxides. Journal of Geophysical Research 86 (B9), 7967–7982.
Stenberg, B., Viscarra Rossel, R.A., Mouazen, A.M., Wetterlind, J., 2010. Visible and near infrared spectroscopy in soil science. Advances in Agronomy 163–215.
Sunshine, J.M., Pieters, C.M., 1993. Estimating modal abundances from the spectra of natural and laboratory pyroxene mixtures using the modified Gaussian model. Journal of Geophysical Research 98 (E5), 9075–9087.
Sunshine, J.M., Pieters, C.M., 1998. Determining the composition of olivine from reflectance spectroscopy. Journal of Geophysical Research 103 (E6), 13675–13688.
Sunshine, J.M., Pieters, C.M., Pratt, S.F., 1990. Deconvolution of mineral absorption bands: an improved approach. Journal of Geophysical Research 95 (B5), 6955–6966.
Swayze, G.A., Clark, R.N., Goetz, A.F.H., Chrien, T.G., Gorelick, N.S., 2003. Effects of spectrometer band pass, sampling, and signal-to-noise ratio on spectral identification using the Tetracorder algorithm. Journal of Geophysical Research — Planets 108 (E9), 5105.
Tscharntke, T., Hochberg, M.E., Rand, T.A., Resh, V.H., Krauss, J., 2007. Author sequence and credit for contributions in multiauthored publications. PLoS Biology 5 (1), e18.
van der Meer, F.D., van der Werff, H.M., van Ruitenbeek, F.J., Hecker, C.A., Bakker, W.H., Noomen, M.F., van der Meijde, M., Carranza, E.J.M., de Smeth, J.B., Woldai, T., 2012. Multi- and hyperspectral geologic remote sensing: a review. International Journal of Applied Earth Observation and Geoinformation 14 (1), 112–128.
Viscarra Rossel, R.A., 2011. Fine-resolution multiscale mapping of clay minerals in Australian soils measured with near infrared spectra. Journal of Geophysical Research 116 (F4), F04023.
Viscarra Rossel, R.A., Walvoort, D.J.J., McBratney, A.B., Janik, L.J., Skjemstad, J.O., 2006. Visible, near infrared, mid infrared or combined diffuse reflectance spectroscopy for simultaneous assessment of various soil properties. Geoderma 131 (1–2), 59–75.
Warell, J., Davidsson, B.J.R., 2010. A Hapke model implementation for compositional analysis of VNIR spectra of Mercury. Icarus 209 (1), 164–178.
Yang, L., Xian, G., Klaver, J.M., Deal, B., 2003. Urban land-cover change detection through sub-pixel imperviousness mapping using remotely sensed data. Photogrammetric Engineering and Remote Sensing 69 (9), 1003–1010.